THE JOURNAL OF BIOLOGICAL CHEMISTRY VOL. 289, NO. 11, pp. 7730–7737, March 14, 2014

Proteasome-dependent Degradation of Transcription Factor Activating Enhancer-binding Protein 4 (TFAP4) Controls Mitotic Division*

Received for publication, January 11, 2014, and in revised form, February 4, 2014 Published, JBC Papers in Press, February 5, 2014, DOI 10.1074/jbc.M114.549535

Sara D'Annibale[‡], Jihoon Kim[‡], Roberto Magliozzi[‡], Teck Yew Low[§¶1], Shabaz Mohammed[§¶1], Albert J. R. Heck[§¶1], and Daniele Guardavaccaro[‡2]

From the [‡]Hubrecht Institute-KNAW and University Medical Center Utrecht, the [§]Biomolecular Mass Spectrometry and Proteomics, Bijvoet Center for Biomolecular Research and Utrecht Institute for Pharmaceutical Sciences, Utrecht University, and [¶]The Netherlands Proteomics Center, 3584 CH Utrecht, The Netherlands

Background: TFAP4 is a transcription factor that controls cell proliferation, stemness and epithelial-mesenchymal transition and is up-regulated in colorectal cancer.
Results: TFAP4 is targeted for degradation by the $SCF^{\beta TrCP}$ ubiquitin ligase. Failure to degrade TFAP4 leads to aberrant mitosis.
Conclusion: TFAP4 degradation is required for the fidelity of mitosis.
Significance: Misregulation of TFAP4 might contribute to genomic instability and tumorigenesis.

TFAP4, a basic helix-loop-helix transcription factor that regulates the expression of a multitude of genes involved in the regulation of cellular proliferation, stemness, and epithelial-mesenchymal transition, is up-regulated in colorectal cancer and a number of other human malignancies. We have found that, during the G_2 phase of the cell division cycle, TFAP4 is targeted for proteasome-dependent degradation by the $SCF^{\beta TrCP}$ ubiquitin ligase. This event requires phosphorylation of TFAP4 on a conserved degron. Expression of a stable TFAP4 mutant unable to interact with βTrCP results in a number of mitotic defects, including chromosome missegregation and multipolar spindles, which eventually lead to the activation of the DNA damage response. Our findings reveal that βTrCP-dependent degradation of TFAP4 is required for the fidelity of mitotic division.

Transcription factor activating enhancer-binding protein 4 (TFAP4)[3] is a ubiquitously expressed basic helix-loop-helix leucine-zipper transcription factor that binds to the consensus E-box sequence 5′-CAGCTG-3′ (1). It has been reported that TFAP4 controls the expression of numerous genes regulating cell proliferation (2, 3). TFAP4 target genes also include stem cell markers such as LGR5 and regulators of epithelial-mesenchymal transition such as SNAIL and E-cadherin (2, 3). Importantly, TFAP4 protein levels have been found elevated in human colorectal, hepatocellular, and gastric carcinoma (3–5). Despite the described role of TFAP4 in cancer, the molecular mechanisms controlling TFAP4 protein levels and the post-translational modifications regulating TFAP4 stability are currently unknown.

In the present study, we identify TFAP4 as a new interactor of the F-box protein βTrCP (β-transducin repeat-containing protein) in a mass spectrometry-based screen aimed at the identification of substrates of $SCF^{\beta TrCP}$, a multisubunit Cullin-RING ubiquitin ligase composed of a cullin scaffold, Cul1, the adaptor protein Skp1, and the RING subunit Rbx1. It is well established that, through its WD40 repeats, βTrCP recognizes a diphosphorylated motif with the consensus DpSGΦ*X*(*X*)pS in which the serine residues are phosphorylated to allow binding to βTrCP (6). Notably, work by several groups has demonstrated that $SCF^{\beta TrCP}$ plays a fundamental role in the regulation of many cellular processes that are related to cancer through targeted destruction of its specific substrates (7, 8).

We also show that during the G_2 phase of the cell cycle, $SCF^{\beta TrCP}$ targets TFAP4 for proteasomal degradation and demonstrate that defective degradation of TFAP4 results in aberrant mitotic divisions and chromosome missegregation, which lead to the activation of the DNA damage checkpoint.

EXPERIMENTAL PROCEDURES

Cell Culture, Synchronization, and Drug Treatment—HeLa, HEK293T, 293GP2, U2OS, hTERT-RPE1, DLD1, and HCT116 cells were maintained in Dulbecco's modified Eagle's medium (Invitrogen) containing 10% fetal calf serum. HeLa and hTERT-RPE1 cells were synchronized at G_1/S by thymidine treatment as described (9). DLD1 cells were synchronized at the G_1/S transition by using FBS-depleted medium for 32 h followed by treatment with aphidicolin (2 μg/ml) for another 24 h. The following drugs were used: nocodazole (0.1 μg/ml) to arrest cells in prometaphase, MG132 (10 μM) to inhibit the proteasome, cycloheximide (100 μg/ml) to block protein synthesis and doxycycline (1 μg/ml) to induce the expression of TFAP4 (wild type or mutants).

* Work in the Guardavaccaro laboratory was supported by the Royal Dutch Academy of Arts and Sciences, the Dutch Cancer Society, the Cancer Genomics Center, and the European Union under Marie Curie Actions (FP7).
[1] Supported by the Netherlands Proteomics Center.
[2] To whom correspondence should be addressed: Hubrecht Institute, Uppsalalaan 8, 3584 CT Utrecht, The Netherlands. Tel.: 31-0-30-212-19-32; Fax: 31-0-30-251-64-64; E-mail: d.guardavaccaro@hubrecht.eu.
[3] The abbreviations used are: TFAP4, transcription factor activating enhancer-binding protein 4; FUCCI, fluorescent ubiquitylation-based cell cycle indicator; RPE1, retinal pigment epithelial; hTERT, human telomerase reverse transcriptase.

Biochemical Methods—Immunoprecipitation and immunoblotting were performed by standard methods and have been described previously (10–12).

Purification of βTrCP2 Interactors—HEK293T cells were transfected with pcDNA3-FLAG-HA-βTrCP2 or pcDNA3-FLAG-HA-βTrCP2(R447A) and treated with 10 μM MG132 for 6 h. Cells were harvested and subsequently lysed in lysis buffer (50 mM Tris-HCl, pH 7.5, 150 mM NaCl, 1 mM EDTA, 0.5% Nonidet P-40, plus protease and phosphatase inhibitors). βTrCP2 was immunopurified with anti-FLAG agarose resin (Sigma-Aldrich). After washing, proteins were eluted by competition with FLAG peptide (Sigma-Aldrich). The eluate was then subjected to a second immunopurification with anti-HA resin (12CA5 monoclonal antibody cross-linked to protein G-Sepharose; Invitrogen) prior to elution in Laemmli sample buffer. The final eluate was separated by SDS-PAGE, and proteins were visualized by Coomassie colloidal blue. Bands were sliced out from the gels and subjected to in-gel digestion. Gel pieces were then reduced, alkylated, and digested according to a published protocol (13). For mass spectrometric analysis, peptides recovered from in-gel digestion were separated with a C18 column and introduced by nano-electrospray into the LTQ Orbitrap XL (Thermo Fisher) with a configuration as described (14). Peak lists were generated from the MS/MS spectra using MaxQuant build (version 1.0.13.13) (15) and then searched against the IPI Human database (version 3.37, 69164 entries) using Mascot search engine (Matrix Science). Carbaminomethylation (+57 Da) was set as fixed modification, and protein N-terminal acetylation and methionine oxidation were set as variable modifications. Peptide tolerance was set to 7 ppm, and fragment ion tolerance was set to 0.5 Da, allowing two missed cleavages with trypsin enzyme. Finally, Scaffold (version Scaffold_3.6.1, Proteome Software, Inc.) was used to validate MS/MS-based peptide and protein identifications. Peptide identifications were accepted if their Mascot scores exceeded 20.

Antibodies—Mouse monoclonal antibodies were from Invitrogen (Cul1), Sigma-Aldrich (FLAG, α-tubulin FITC conjugate), Santa Cruz Biotechnology (actin), BD Biosciences (β-catenin), Covance (HA), and Novus Biologicals (TFAP4). Rabbit polyclonal antibodies were from Cell Signaling (βTrCP1), Bethyl Laboratories (PDCD4), Millipore (REST, phospho-histone H3 (Ser-10)), Sigma-Aldrich (FLAG), Santa Cruz Biotechnology (cyclin A, HA, and Skp1).

Plasmids—TFAP4 mutant was generated using the QuikChange site-directed mutagenesis kit (Stratagene). For retrovirus production, both wild type TFAP4 and the non-degradable TFAP4 mutant were subcloned into the retroviral vector LZRSpBMN-GFP. For producing lentiviruses, both wild type TFAP4 and the TFAP4 mutant were subcloned into the lentiviral vector pHAGE2-EF1α. Enhanced green fluorescent protein-labeled histone H2B was cloned into pEGFP-N1 vector. To generate the fluorescent ubiquitylation-based cell cycle indicator (FUCCI) cells, the constructs pCSII-EF-mKO2-hCdt1(30/120) and pCSII-EF-mAG-hGEM(1/110) were used. For stable transfection, wild type TFAP4 and TFAP4(E135A/S139A) were subcloned into pcDNA 4/TO inducible vector. All cDNAs were sequenced.

Transient Transfections and Retrovirus- and Lentivirus-mediated Gene Transfer—HEK293T cells were transfected using the calcium phosphate method as described (11). HCT116 cells were transfected with Lipofectamine according to the manufacturer's instructions. Retrovirus-mediated gene transfer was described previously (11, 12). For lentivirus production, HEK293T cells were co-transfected with pHAGE2-EF1α and packaging vectors by using polyethylenimine. Virus-containing medium was collected 48 h after transfection and supplemented with 8 μg/ml polybrene. Cells were incubated with virus-containing medium for 6 h for 2 consecutive days.

Gene Silencing by Small Interfering RNA—The sequences and validation of the oligonucleotides corresponding to βTrCP1 and βTrCP2 were described previously (9, 16, 17). Cells were transfected with the oligonucleotides twice (24 and 48 h after plating) using Oligofectamine (Invitrogen) according to the manufacturer's recommendations. Forty-eight hours after the last transfection, lysates were prepared and analyzed by SDS-PAGE and immunoblotting.

In Vitro Ubiquitylation Assay—$SCF^{\beta TrCP}$-mediated ubiquitylation assays were described previously (12, 18). Briefly, TFAP4 ubiquitylation was performed in a volume of 10 μl containing βTrCP-TFAP4 immunocomplexes, 50 mM Tris, pH 7.6, 5 mM $MgCl_2$, 0.6 mM DTT, 2 mM ATP, 2 μl of *in vitro*-translated unlabeled βTrCP1, 1.5 ng/μl E1 (Boston Biochem), 10 ng/μl Ubc3, 2.5 μg/μl ubiquitin (Sigma), and 1 μM ubiquitin aldehyde. The reactions were incubated at 30 °C for the indicated times and analyzed by immunoblotting.

Phosphorylation Analysis by Mass Spectrometry—Samples were reduced with 10 mM DTT for 30 min at 60 °C, followed by addition of iodoacetamide to 20 mM followed by a 30-min incubation in the dark at room temperature. The first digestion was performed using Lys-C for 4 h at 37 °C. Subsequently, the digest was diluted 5-fold using 50 mM ammonium bicarbonate to a final urea concentration of <2 M, and a second digestion with trypsin was performed overnight at 37 °C. Finally, the digestion was quenched by addition of formic acid to a final concentration of 0.1% (v/v). The resulting solution was desalted using 200 mg Sep-Pak C18 cartridges (Waters Corp.), lyophilized and reconstituted in 10% formic acid. LC-MS/MS was performed with both collision-induced dissociation and electron transfer dissociation in the form of data-dependent decision tree (19, 20). MS spectra to peptide sequence assignment is performed with Proteome Discoverer (version 1.3), with MASCOT (version 2.3) as search engine and the localization of phosphorylated sites was evaluated with PhosphoRS (version 2) (21).

Immunofluorescence—Cells were plated and cultured on coverslips coated with polylysine (Sigma-Aldrich) with complete medium. Cells were fixed and permeabilized in 100% methanol at −20 °C for 10 min and then incubated with the primary FITC-conjugated antibody for 1 h at room temperature in 0.5% Tween 20 in PBS (TBST). Cells were washed three times in 0.5% TBST. Hoechst 33342 (Sigma-Aldrich) was included to detect the nuclei. Slides were mounted by using Vectashield mounting media (Vector Labs).

Live Cell Imaging—Cells were plated and cultured in 24-well plates in complete medium. Microscope was equipped with an

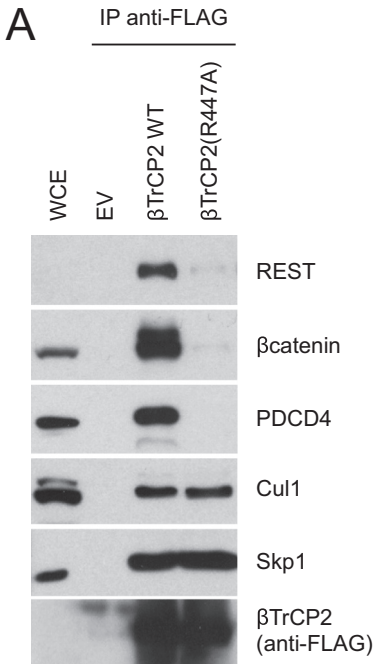

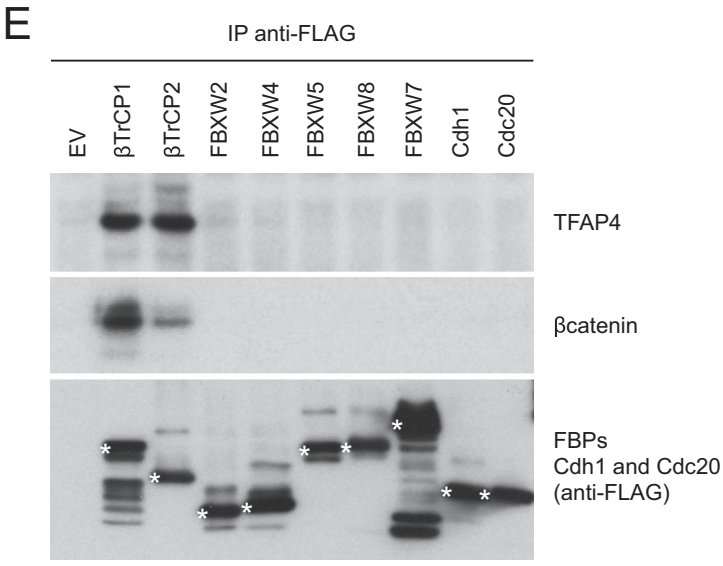

B

	βTrCP2 WT	βTrCP2(R447A)
Unique peptides	6	0
Unique spectra	8	0
Total spectra	10	0
Identified aa/total aa	72/338	0/338
% coverage	21	0
Peptide #1	(R)AVIVKPVR(S)	-
Peptide #2	(K)VPSLQHFR(K)	-
Peptide #3	(R)LLQQNTQLK(R)	-
Peptide #4	(K)VIAQQVQLQQQQEQVR(L)	-
Peptide #5	(R)MQSINAGFQSLK(T)	-
Peptide #6	(R)QNLDTIVQAIQHIEGTQEK(Q)	-

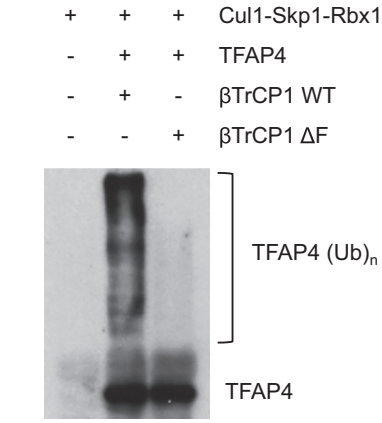

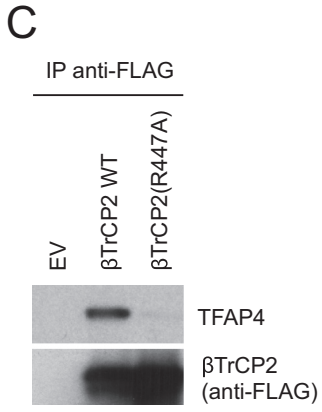

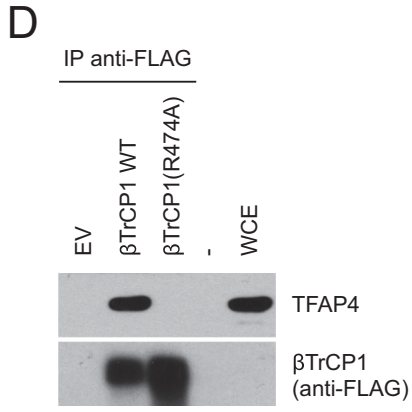

F

Protein	Protein ID	Unique peptides	Total spectra
TFAP4	Q01664	27	231
βTrCP2	Q9UKB1	21	30
βTrCP1	Q9Y297	8	9
Skp1	P63208	6	8
Cul1	Q13616	3	3

FIGURE 1. **Immunopurification of βTrCP2 and identification of TFAP4 as a putative substrate of SCF^{βTrCP}.** *A*, FLAG-tagged wild type βTrCP2 or the βTrCP2(R447A) mutant were expressed in HEK293T cells. Forty-eight hours after transfection, cells were treated for 6 h with the proteasome inhibitor MG132 and then collected and lysed. Whole cell extracts (*WCE*) were immunoprecipitated with anti-FLAG resin and immunoblotted with antibodies for the indicated proteins. *B*, list of unique peptides identified in wild type βTrCP2 and βTrCP2(R447A) immunopurifications. *C* and *D*, HEK293T cells were transfected with an empty vector (*EV*) or the indicated F-box proteins. Forty-eight hours after transfection, cells were treated for 6 h with the proteasome inhibitor MG132 and then collected and lysed. Whole cell extracts were immunoprecipitated with anti-FLAG resin and immunoblotted with anti-TFAP4 and anti-FLAG antibodies. *E*, HEK293T cells were transfected with an empty vector, the indicated FLAG-tagged F-box proteins (*FBPs*), CDH1, or CDC20. Cells were treated as in *A*. Whole cell extracts were immunoprecipitated with anti-FLAG resin and immunoblotted with antibodies specific for the indicated proteins. *F*, list of proteins identified in the immunopurification of FLAG-HA epitope-tagged TFAP4. The number of unique peptides and total spectra recovered for the indicated proteins are shown. *G*, *in vitro* ubiquitylation assay of TFAP4 by immunopurified βTrCP. HEK293T cells were transfected with TFAP4, Skp1, Cul1, and Rbx1 in the absence or presence of either FLAG-tagged βTrCP1 or a FLAG-tagged βTrCP1(ΔF-box) mutant. After immunopurification with an anti-FLAG resin, *in vitro* ubiquitylation of TFAP4 was performed. Samples were analyzed by immunoblotting with an anti-TFAP4 antibody.

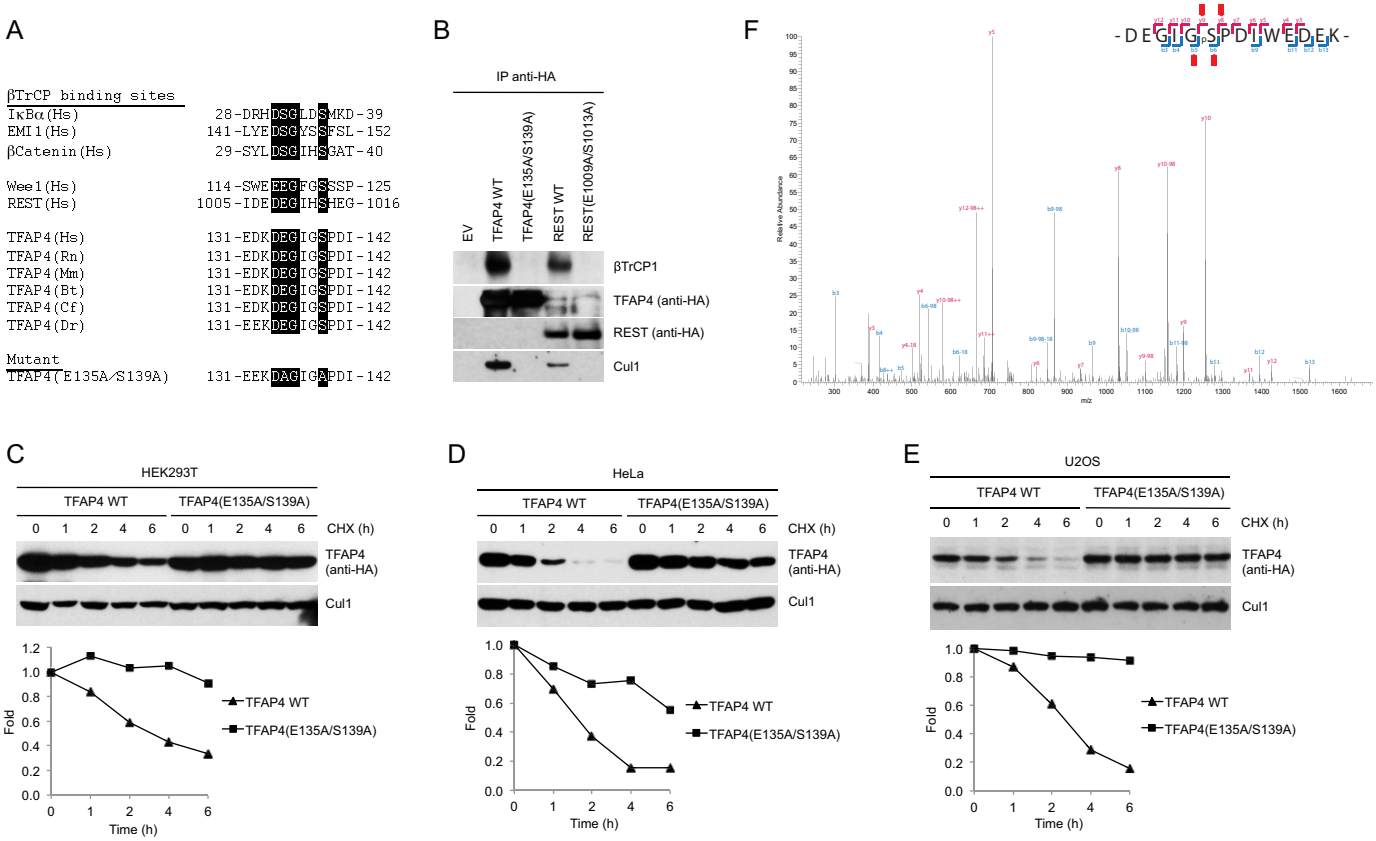

FIGURE 2. **A conserved phosphodegron is required for the binding of TFAP4 to βTrCP.** *A*, schematic representation of the βTrCP-binding motifs in previously reported substrates of βTrCP aligned with the candidate phosphodegron in TFAP4 orthologs. The amino acidic sequence of the double mutant is shown (*bottom*). *B*, TFAP4 Glu-135 and Ser-139 are required for the interaction of TFAP4 with βTrCP1. HEK293T cells were transfected with the indicated HA-tagged proteins. Whole-cell extracts were subjected to immunoprecipitation (*IP*) with HA-resin, followed by immunoblotting with antibodies specific for the indicated proteins. Immunoprecipitations of the known βTrCP substrate REST (wild type and E1009A/S1013A) are shown as additional controls. *C–E*, HA-tagged wild type TFAP4 and TFAP4(E135A/S139A) were expressed in HEK293T (*C*), HeLa (*D*), and U2OS (*E*) cells. Cells were treated with cycloheximide (*CHX*) for the indicated times and collected. Proteins were analyzed by immunoblotting with an anti-HA antibody to detect TFAP4 or with an anti-Cul1 antibody to show loading normalization. The graphs show the quantification of TFAP4 abundance relative to the amount at time 0. *F*, FLAG-HA-tagged βTrCP was immunoprecipitated from HEK293T cells and analyzed by mass spectrometry. The ion fragmentation spectrum is shown. The TFAP4 tryptic peptide DEGIGSPDIWEDEK spanning the phosphodegron was found phosphorylated on Ser-139. As shown, peptide sequences can be explained by their respective collision-induced dissociation MS/MS spectra, including phospho-Ser-139. The diagnostic daughter ions are highlighted with *red arrows*. *EV*, empty vector; *Hs*, *Homo sapiens*; *Rn*, *Rattus norvegicus*; *Mm*, *Mus musculus*; *Bt*, *Bos taurus*; *Cf*, *Canis familiaris*; *Dr*, *Danio rerio*.

incubating chamber at 37 °C and a CO_2 supply. Images were taken at 10-min intervals over 24 h.

RESULTS

Structural studies have shown that arginine 474 in the WD40 β-propeller of βTrCP1 contacts the DpSGΦ*X*(*X*)pS destruction motif of βTrCP substrates (22). It has been also reported that the βTrCP1(R474A) mutant is not able to promote polyubiquitylation of its substrate IκBα in an *in vitro* ubiquitylation assay (22). We confirmed that the equivalent βTrCP2 mutant (βTrCP2(R447A)) does not bind to previously established βTrCP substrates such as β-catenin, REST (repressor element-1-silencing transcription factor), and PDCD4 (programmed cell death-4), while retaining the ability to interact with the SCF subunits Cul1 and Skp1 (Fig. 1*A*). We took advantage of these properties of βTrCP and used a differential immunopurification strategy followed by mass spectrometry analysis to identify novel substrates of $SCF^{\beta TrCP}$. We expressed either wild type βTrCP2 or the βTrCP2(R447A) mutant (both FLAG-HA epitope-tagged at the N terminus) in HEK293T cells and purified βTrCP2 immunoprecipitates, which were then analyzed by mass spectrometry. Six unique peptides corresponding to the basic helix-loop-helix leucine zipper transcription factor TFAP4 were recovered in wild type βTrCP2 immunoprecipitates, but not in βTrCP2(R447A) immunopurifications (Fig. 1*B*).

To confirm the binding between βTrCP and TFAP4, we immunoprecipitated FLAG-tagged wild type βTrCP2 and assessed its binding to endogenous TFAP4 by immunoblotting. As shown in Fig. 1*C*, wild type βTrCP2, but not the βTrCP2(R447A) mutant, coimmunoprecipitated with endogenous TFAP4. Similar results were obtained with βTrCP1 (Fig. 1*D*).

To assess the specificity of the βTrCP-TFAP4 interaction, we immunoprecipitated a number of FLAG epitope-tagged F-box proteins as well as the related proteins Cdh1 and Cdc20 from HEK293T cells and analyzed their ability to pull down endogenous TFAP4. βTrCP1 and βTrCP2 coimmunoprecipitated with endogenous TFAP4 (Fig. 1*E*), whereas other members of the FBXW family of F-box proteins, FBXW2, FBXW4, FBXW5, FBXW7, FBXW8, or the APC/C activators Cdh1 and Cdc20 (also containing WD40 repeats) did not.

When we immunopurified FLAG-HA epitope-tagged TFAP4, we recovered unique peptides corresponding to subunits of

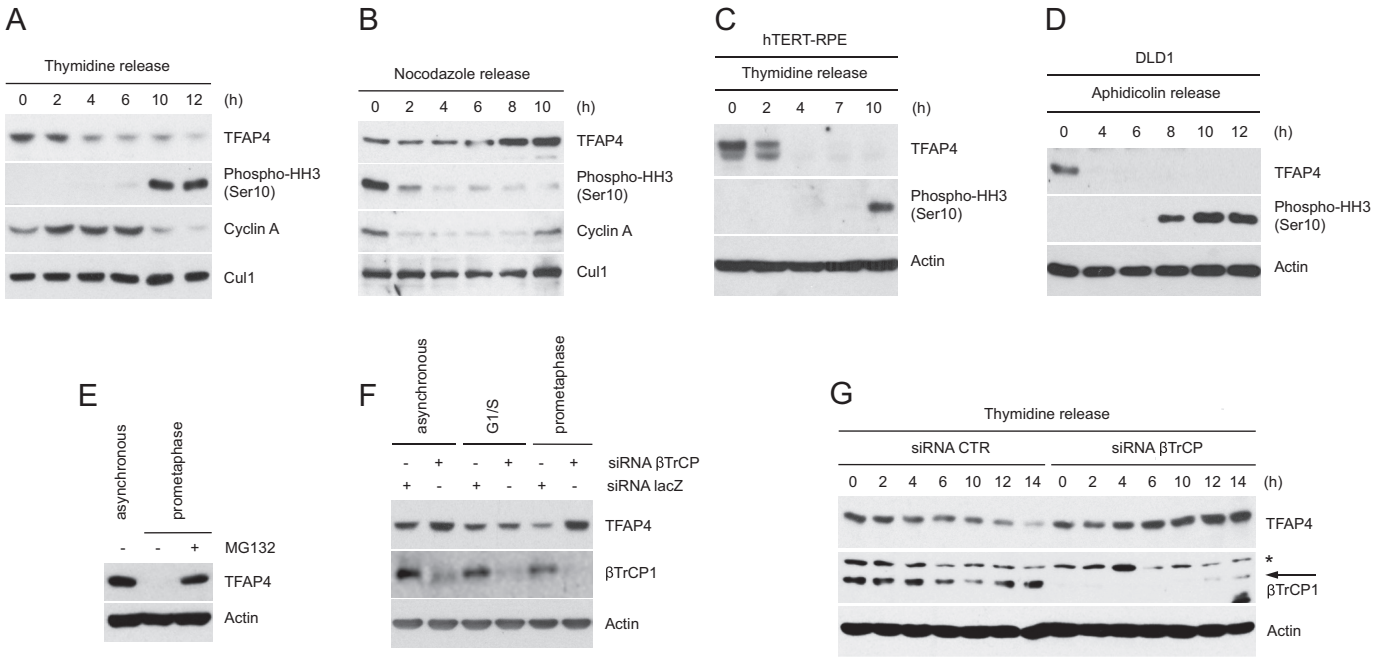

FIGURE 3. **TFAP4 is degraded during the G_2 phase of the cell cycle.** *A* and *B*, HeLa cells were synchronized at the G_1/S transition by double thymidine block and then released in fresh medium containing nocodazole (*A*) or in mitosis by the nocodazole block-and-release procedure (*B*). *C*, hTERT-RPE1 cells were synchronized at G_1/S by double thymidine block and released into nocodazole containing medium. *D*, to synchronize DLD1 cells at G_1/S, cells were first serum starved (32 h) and then incubated in serum-containing medium in the presence of aphidicolin for 24 h. Cells were then released from the G_1/S block in nocodazole-containing medium. Cells were collected at the indicated times, lysed, and analyzed by immunoblotting with the indicated antibodies. Actin or Cul1 were used as loading controls. *E*, asynchronously growing or nocodazole-treated HeLa cells were collected and analyzed by immunoblotting with antibodies for the indicated proteins. When indicated, cells were treated with the proteasome inhibitor MG132 for 6 h. *F*, HeLa cells were transfected with siRNA corresponding to a non-relevant mRNA (control siRNA) or to βTrCP mRNA. Twelve hours after transfection, cells were either left untreated of treated with thymidine (to synchronize them at G_1/S) or nocodazole (to synchronize them in prometaphase). Cells were collected, lysed, and analyzed by immunoblotting. *G*, HeLa cells, transfected as in *F*, were synchronized as in *A*. Cells were then collected at the indicated time points and analyzed by immunoblotting with antibodies for the indicated proteins. Actin levels are shown as loading control. The *asterisk* indicates a nonspecific band.

$SCF^{\beta TrCP}$, *i.e.* βTrCP1 (8), βTrCP2 (21), Skp1 (6), and Cul1 (Fig. 1*F*) (3), further supporting the interaction between TFAP4 and $SCF^{\beta TrCP}$.

To test whether $SCF^{\beta TrCP}$ is directly responsible for the ubiquitylation of TFAP4, we reconstituted TFAP4 ubiquitylation *in vitro*. Immunopurified wild type βTrCP1, but not βTrCP1(ΔF-box), an inactive mutant that lacks the F-box domain, triggered efficient ubiquitylation of TFAP4 *in vitro* (Fig. 1*G*).

Substrates of $SCF^{\beta TrCP}$ contain a conserved DpSGΦ*X*(*X*)pS degron that mediates the interaction with βTrCP (6, 7, 22). TFAP4 has a modified motif in which the first serine residue is replaced by glutamic acid as other established substrates of $SCF^{\beta TrCP}$ (Fig. 2*A*) (11, 23, 24). We generated a mutant TFAP4 protein in which glutamic acid 135 and serine 139 were substituted with alanine (Fig. 2*A*) and examined its ability to interact with βTrCP. The TFAP4(E135A/S139A) mutant did not bind endogenous βTrCP in immunoprecipitation experiments (Fig. 2*B*) and was markedly stabilized as demonstrated by half-life experiments carried out in various cell lines (Fig. 2, *C–E*).

To test whether Ser-139 is phosphorylated in cultured cells, we purified βTrCP2 from HEK293T cells treated with the proteasome inhibitor MG132 and analyzed the phosphorylation of co-immunoprecipitating TFAP4 by tryptic digestion followed by phosphopeptide enrichment and LC-MS/MS. Analysis of the recovered TFAP4 phosphopeptides demonstrated that Ser-139 is phosphorylated in cells (Fig. 2*F*).

As it has been reported that TFAP4 controls the expression of many cell cycle regulators (2, 3), we hypothesized that the protein levels of TFAP4 might oscillate during cell cycle progression. To test this hypothesis, we analyzed by immunoblotting the abundance of TFAP4 throughout the cell cycle. HeLa cells were synchronized at the G_1/S transition by double thymidine block before releasing them into fresh medium (to analyze TFAP4 protein levels in the following S, G_2, and M phases) and in mitosis by the nocodazole block-and-release procedure (Fig. 3, *A* and *B*). Synchronization was monitored by immunodetection of cyclin A (an S/G_2 phase protein) and phospho-histone H3 (a mitotic marker) as well as by flow cytometry (data not shown). We found that the abundance of TFAP4 oscillates during the cell cycle. The levels of TFAP4 decreased in early G_2 (at a time when the levels of cyclin A, which is degraded in early mitosis, were still elevated), remained low in mitosis and in the following G_1, and increased at G_1/S preceding cyclin A up-regulation. Similar kinetics of TFAP4 decrease in early G_2 was observed in other cell types such as non-transformed hTERT-immortalized retinal pigment epithelial (hTERT-RPE1) cells (Fig. 3*C*) and DLD1 cells (Fig. 3*D*). The proteasome inhibitor MG132 prevented the disappearance of TFAP4 in HeLa cells arrested in prometaphase, indicating that the degradation of TFAP4 in G_2 is mediated by the proteasome (Fig. 3*E*).

To test whether the degradation of TFAP4 is mediated by βTrCP, we silenced the expression of both βTrCP1 and βTrCP2 by RNAi (18, 25) in HeLa cells. Fig. 3*F* shows that the knockdown of βTrCP caused accumulation of TFAP4 in prometaphase, whereas it had no effect in cells arrested at G_1/S and a moderate effect in asynchronous cells.

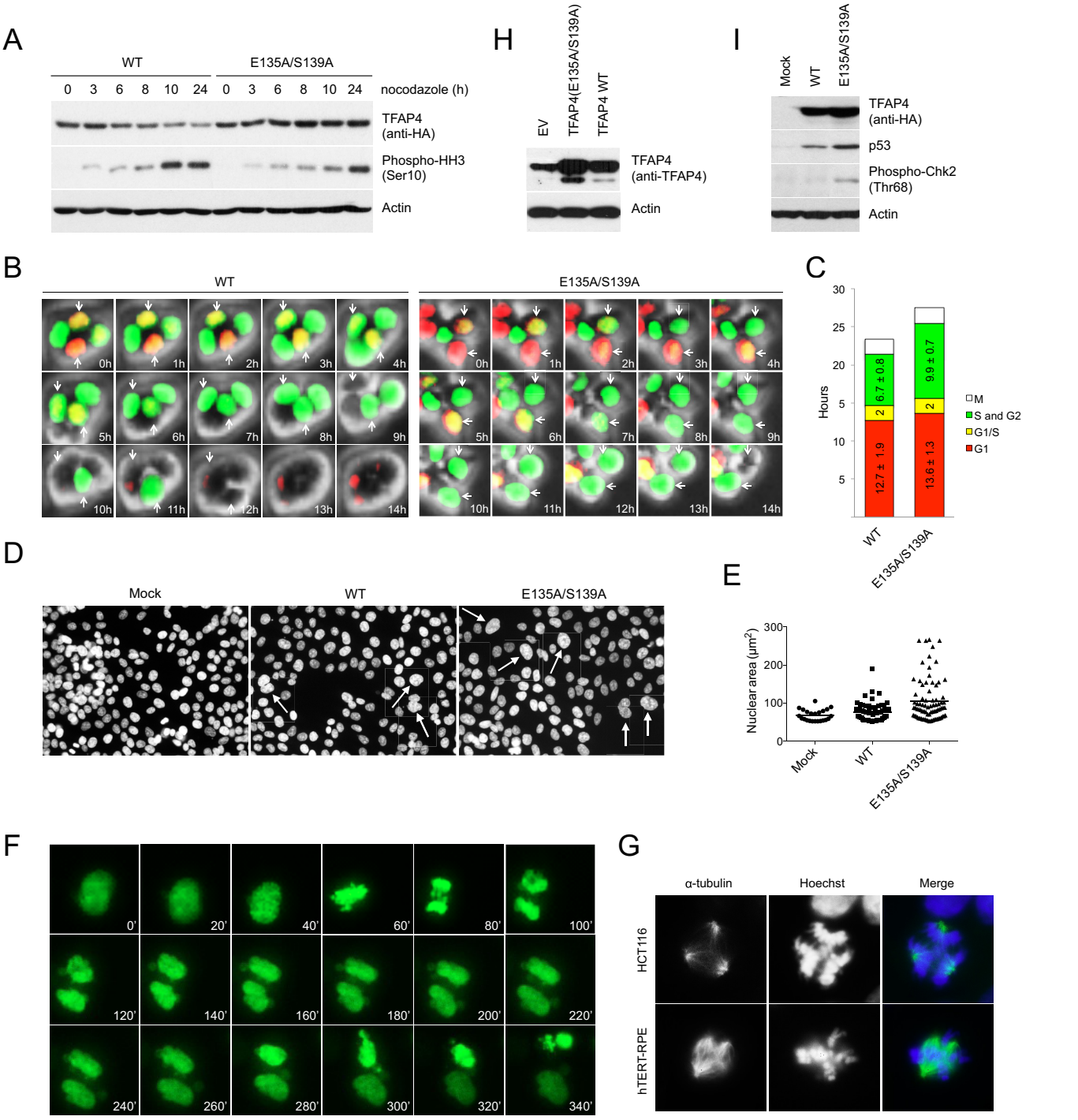

FIGURE 4. **Expression of the degradation-resistant TFAP4 mutant results in delayed G_2 progression, nuclear atypia, chromosome missegregation, and mitotic spindle aberrations.** *A*, cells expressing wild type TFAP4 or the TFAP4(E135A/S139A) mutant were treated with nocodazole for the indicated times. Cells were lysed and analyzed by immunoblotting with antibodies for the indicated proteins. *B*, HCT116 cells, transduced with FUCCI vectors and expressing either wild type TFAP4 or the non-degradable TFAP4(E135A/S139A) mutant, were analyzed by time-lapse imaging. Phase contrast images and fluorescent images using GFP and rhodamine filters were taken every 10 min. Selected time points (60-min interval) are shown. *C*, quantification of the length of the G_1 (*red*), G_1/S (*yellow*) and S/G_2 (*green*) phases of cells shown in *B*. Average values (± S.D.) are indicated. *D* and *E*, HCT116 control cells, or expressing either wild type TFAP4 or TFAP4(E135A/S139A), were fixed and stained with the Hoechst 33342 dye. *White arrows* indicate enlarged lobulated nuclei. Quantification of the nuclear size is shown in *E*. *Horizontal lines* represent the mean. $p < 0.001$ (Student's *t* test). *F*, HCT116 cells, transduced with histone H2B-GFP and expressing either wild type TFAP4 or the degradation-resistant TFAP4(E135A/S139A) mutant, were filmed for 24 h. Still frames showing an example of aberrant mitotic divisions occurring in cells expressing TFAP4(E135A/S139A) are shown. *G*, HCT116 (*top*) and hTERT-RPE1 cells (*bottom*), expressing either wild type TFAP4 or TFAP4(E135A/S139A), were fixed and stained with anti-α-tubulin antibody (to visualize mitotic spindles) and Hoechst 33342 (to visualize DNA). Examples of mitotic spindle aberrations in cells expressing TFAP4(E135A/S139A) are shown. *H*, moderate ectopic expression of TFAP4 in cells. Cells were mock-transduced or transduced with retroviruses expressing HA-tagged wild type TFAP4 or the TFAP4(E135A/S139A) mutant. Cells were collected and lysed. Whole cell extracts were analyzed by immunoblotting. An anti-TFAP4 antibody was employed to detect endogenous (*first lane*) and both endogenous and exogenous (*second* and *third lane*) levels of TFAP4. Actin is shown as a loading control. *I*, HCT116 control cells, or expressing either wild type TFAP4 or TFAP4(E135A/S139A), were lysed and analyzed by immunoblotting with antibodies specific for the indicated proteins. Actin is shown as a loading control. *EV*, empty vector.

To pinpoint when βTrCP targets TFAP4 for proteasome-dependent degradation, βTrCP-silenced cells were released from a thymidine block and collected at different time points. As shown in Fig. 3*G*, the knockdown of βTrCP prevented the destruction of TFAP4 occurring ~4–6 h after cells were released from the thymidine block.

To study the function of the βTrCP-mediated degradation of TFAP4 during cell cycle, we transduced cells with lentiviruses expressing wild type TFAP4 and the degradation-resistant TFAP4(E135A/S139A) mutant. Cells approaching mitosis were then analyzed by immunoblotting (Fig. 4*A*). As expected, although levels of wild type TFAP4 decreased as cells moved toward mitosis, levels of the TFAP4(E135A/S139A) mutant remained unchanged. Moreover, compared with cells expressing wild type TFAP4, cells expressing the non-degradable TFAP4 mutant displayed a slower kinetics of mitotic entry as indicated by the phosphorylation of histone H3 on Ser-10.

To examine whether the late mitotic entry of cells expressing the non-degradable TFAP4 mutant was caused, at least in part, by a delay in G_2 progression, we employed FUCCI (26) live cell imaging. This system is based on the expression of both a red (RFP) and green (GFP) fluorescent protein fused to Cdt1 and geminin, respectively. Based on the fact that Cdt1-RFP is targeted for degradation in G2 by the SCF^{Skp2} ubiquitin ligase and geminin-GFP is degraded in late M and early G_1 by APC/C^{Cdh1}, cells are red in G_1, become yellow upon entry in S phase (where both fusion proteins are present), are green throughout S and G_2, and are colorless at the end of mitosis. We generated stable transfectants of HCT116-FUCCI cells in which the expression of TFAP4 (wild type or TFAP4(E135A/S139A)) could be pulsed-induced by doxycycline. These cells were then analyzed by live cell imaging. As shown in Fig. 4, *B* and *C*, cells expressing wild type TFAP4 and the TFAP4(E135A/S139A) mutant displayed a similar Cdt1-positive G_1 phase; however, cells expressing the non-degradable TFAP4(E135A/S139A) mutant showed a prolonged geminin-positive S/G_2 (9.9 h) when compared with cells expressing wild type TFAP4 (6.8 h).

In the course of our experiments, we observed that the expression of the non-degradable TFAP4(E135A/S139A) mutant in HCT116 cells, which have a relatively stable karyotype, resulted in notable nuclear atypia, including lobulated and enlarged nuclei (Fig. 4, *D* and *E*). This phenotype becomes increasingly penetrant with longer time of doxycycline treatment (which triggers the expression of wild type TFAP4 or TFAP4(E135A/S139A)), eventually occurring in virtually all cells. Notably, although less pronounced, nuclear atypia was also present in cells overexpressing wild type TFAP4.

To test whether these cellular abnormalities were caused by defective mitotic divisions, we expressed wild type TFAP4 and the non-degradable TFAP4(E135A/S139A) mutant in HCT116 cells expressing enhanced green fluorescent protein-labeled histone H2B, which were then analyzed by time-lapse microscopy. We found that cells expressing TFAP4(E135A/S139A) displayed chromosome missegregation (Fig. 4*F*). The percentage of mitotic cells with chromosome missegregation was 28% ($n = 100$) for the non-degradable TFAP4 and 14% ($n = 100$) for wild type TFAP4. In addition, HCT116 cells expressing TFAP4(E135A/S139A) displayed a number of mitotic spindle abnormalities, including the formation of multipolar spindles, as judged by α-tubulin and Hoechst staining. The percentage of mitotic cells with multipolar spindles was ~30% ($n = 300$) for the degradation-resistant TFAP4 mutant and close to 10% ($n = 300$) for wild type TFAP4. Examples of mitoses with multipolar spindles in HCT116 and hTERT-RPE1 cells are shown in Figs. 4*G*.

Notably, the expression of the degradation-resistant TFAP4(E135A/S139A) mutant intensified the phenotypes observed in cells expressing wild type TFAP4, likely as a result of the persistence of TFAP4 expression in G_2 rather than TFAP4 overexpression. In fact, the same mitotic aberrations and nuclear defects were also observed when TFAP4(E135A/S139A) was expressed at moderate levels in a retroviral vector (Fig. 4*H*).

It has been shown that missegregating chromosomes are often damaged during cytokinesis, triggering a DNA double-strand break response (27). The observed chromosome segregation errors in cells expressing the degradation-resistant TFAP4 mutant (Fig. 4, *D*–*G*), as well as their slower kinetics of mitotic entry and prolonged progression through G2 (Fig. 4, *A*–*C*) prompted us to test whether failure to degrade TFAP4 results in the activation of the G_2 DNA damage checkpoint. As shown in Fig. 4*I*, expression of the TFAP4(E135A/S139A) mutant leads to accumulation of p53 and phosphorylation of Chk2 on threonine 68, two markers of damaged DNA, indicating that stabilizing mutations of TFAP4 induce the activation of the DNA damage response.

DISCUSSION

In sum, we have shown that during the G_2 phase of the cell division cycle, TFAP4 is targeted for degradation by the $SCF^{\beta TrCP}$ ubiquitin ligase. Notably, a genome-wide characterization of TFAP4-controlled genes by mRNA profiling and DNA binding analysis has been recently reported (2) and hundreds of TFAP4 target genes, which are either induced or repressed by TFAP4, have been identified. Gene ontology analysis revealed that genes encoding cell cycle regulators were highly enriched among the TFAP4-regulated genes suggesting that βTrCP-dependent degradation TFAP4 in G_2 is required to modulate the expression of a multitude of genes controlling cell cycle progression.

Evidence for overexpression of TFAP4 in colorectal, hepatocellular, and gastric carcinoma has been shown previously (3–5). Our study, demonstrating that overexpression of wild type TFAP4 and, more dramatically, the non-degradable TFAP4 mutant, leads to aberrant mitotic division, suggests a mechanism by which the misregulation of TFAP4 observed in cancer may contribute to genomic instability and tumor progression. As mutations in c-MYC, a direct activator of TFAP4, are frequent in cancer, an analysis of the occurrence of stabilizing and/or activating mutations in the TFAP4 gene in human tumors should be warranted.

Acknowledgments—We thank Z. Ping, R. Lim, and the Hubrecht Imaging Center (HIC) for contributions and A. Miyawaki for the FUCCI vectors.

REFERENCES

1. Jung, P., and Hermeking, H. (2009) The c-MYC-AP4-p21 cascade. *Cell Cycle* **8,** 982–989
2. Jackstadt R., Röh, S., Neumann, J., Jung, P., Hoffmann, R., Horst, D., Berens, C., Bornkamm, G. W., Kirchner, T., Menssen, A., and Hermeking, H. (2013) AP4 is a mediator of epithelial-mesenchymal transition and metastasis in colorectal cancer. *J. Exp. Med.* **210,** 1331–1350
3. Jung, P., Menssen, A., Mayr, D., and Hermeking, H (2008) AP4 encodes a c-MYC-inducible repressor of p21. *Proc. Natl. Acad. Sci. U.S.A.* **105,** 15046–15051
4. Hu, B. S., Zhao, G., Yu, H. F., Chen, K., Dong, J. H., and Tan, J. W. (2013) High expression of AP-4 predicts poor prognosis for hepatocellular carcinoma after curative hepatectomy. *Tumour Biol.* **34,** 271–276
5. Xinghua, L., Bo, Z., Yan, G., Lei, W., Changyao, W., Qi, L., Lin, Y., Kaixiong, T., Guobin, W., and Jianying, C. (2012) The overexpression of AP-4 as a prognostic indicator for gastric carcinoma. *Med. Oncol.* **29,** 871–877
6. Frescas, D., and Pagano, M. (2008) Deregulated proteolysis by the F-box proteins SKP2 and β-TrCP: tipping the scales of cancer. *Nat. Rev. Cancer* **8,** 438–449
7. Cardozo, T., and Pagano, M. (2004) The SCF ubiquitin ligase: insights into a molecular machine. *Nat. Rev. Mol. Cell Biol.* **5,** 739–751
8. Nakayama, K. I., and Nakayama, K. (2006) Ubiquitin ligases: cell-cycle control and cancer. *Nat. Rev. Cancer* **6,** 369–381
9. Guardavaccaro, D., Kudo, Y., Boulaire, J., Barchi, M., Busino, L., Donzelli, M., Margottin-Goguet, F., Jackson, P. K., Yamasaki, L., and Pagano, M. (2003) Control of meiotic and mitotic progression by the F box protein β-Trcp1 *in vivo*. *Dev. Cell* **4,** 799–812
10. Ping, Z., Lim, R., Bashir, T., Pagano, M., and Guardavaccaro, D. (2012) APC/C (Cdh1) controls the proteasome-mediated degradation of E2F3 during cell cycle exit. *Cell Cycle* **11,** 1999–2005
11. Guardavaccaro, D., Frescas, D., Dorrello, N. V., Peschiaroli, A., Multani, A. S., Cardozo, T., Lasorella, A., Iavarone, A., Chang, S., Hernando, E., and Pagano, M. (2008) Control of chromosome stability by the β-TrCP-REST-Mad2 axis. *Nature* **452,** 365–369
12. Dorrello, N. V., Peschiaroli, A., Guardavaccaro, D., Colburn, N. H., Sherman, N. E., and Pagano, M. (2006) S6K1- and βTRCP-mediated degradation of PDCD4 promotes protein translation and cell growth. *Science* **314,** 467–471
13. Shevchenko, A., Wilm, M., Vorm, O., and Mann, M. (1996) Mass spectrometric sequencing of proteins silver-stained polyacrylamide gels. *Anal. Chem.* **68,** 850–858
14. Raijmakers, R., Berkers, C. R., de Jong, A., Ovaa, H., Heck, A. J., and Mohammed, S. (2008) Automated online sequential isotope labeling for protein quantitation applied to proteasome tissue-specific diversity. *Mol. Cell Proteomics* **7,** 1755–1762
15. Cox, J., and Mann, M. (2008) MaxQuant enables high peptide identification rates, individualized p.p.b.-range mass accuracies and proteome-wide protein quantification. *Nat. Biotechnol.* **26,** 1367–1372
16. Peschiaroli, A., Dorrello, N. V., Guardavaccaro, D., Venere, M., Halazonetis, T., Sherman, N. E., and Pagano, M. (2006) SCFβTrCP-mediated degradation of Claspin regulates recovery from the DNA replication checkpoint response. *Mol. Cell* **23,** 319–329
17. Magliozzi, R., Low, T. Y., Weijts, B. G., Cheng, T., Spanjaard, E., Mohammed, S., van Veen, A., Ovaa, H., de Rooij, J., Zwartkruis, F. J., Bos, J. L., de Bruin, A., Heck, A. J., and Guardavaccaro, D. (2013) Control of epithelial cell migration and invasion by the IKKβ- and CK1α-mediated degradation of RAPGEF2. *Dev. Cell* **27,** 574–585
18. Kruiswijk, F., Yuniati, L., Magliozzi, R., Low, T. Y., Lim, R., Bolder, R., Mohammed, S., Proud, C. G., Heck, A. J., Pagano, M., and Guardavaccaro, D. (2012) Coupled activation and degradation of eEF2K regulates protein synthesis in response to genotoxic stress. *Sci. Signal.* **5:** ra40
19. Frese, C. K., Altelaar, A. F., Hennrich, M. L., Nolting, D., Zeller, M., Griep-Raming, J., Heck, A. J., and Mohammed, S. (2011) Improved peptide identification by targeted fragmentation using CID, HCD and ETD on an LTQ-Orbitrap Velos. *J. Proteome Res.* **10,** 2377–2388
20. Swaney, D. L., McAlister, G. C., and Coon, J. J. (2008) Decision tree-driven tandem mass spectrometry for shotgun proteomics. *Nat. Methods* **5,** 959–964
21. Taus, T., Köcher, T., Pichler, P., Paschke, C., Schmidt, A., Henrich, C., and Mechtler, K. (2011) Universal and confident phosphorylation site localization using phosphoRS. *J. Proteome Res.* **10,** 5354–5362
22. Wu, G., Xu, G., Schulman, B. A., Jeffrey, P. D., Harper, J. W., and Pavletich, N. P. (2003) Structure of a β-TrCP1-Skp1-β-catenin complex: destruction motif binding and lysine specificity of the SCF(β-TrCP1) ubiquitin ligase. *Mol. Cell* **11,** 1445–1456
23. Watanabe, N., Arai, H., Nishihara, Y., Taniguchi, M., Watanabe, N., Hunter, T., and Osada, H. (2004) M-phase kinases induce phospho-dependent ubiquitination of somatic Wee1 by SCFβ-TrCP. *Proc. Natl. Acad. Sci. U.S.A.* **101,** 4419–4424
24. Kanemori, Y., Uto, K., and Sagata, N. (2005) β-TrCP recognizes a previously undescribed nonphosphorylated destruction motif in Cdc25A and Cdc25B phosphatases. *Proc. Natl. Acad. Sci. U.S.A.* **102,** 6279–6284
25. Busino, L., Donzelli, M., Chiesa, M., Guardavaccaro, D., Ganoth, D., Dorrello, N. V., Hershko, A., Pagano, M., and Draetta, G. F. (2003) Degradation of Cdc25A by β-TrCP during S phase and in response to DNA damage. *Nature* **426,** 87–91
26. Sakaue-Sawano, A., Kurokawa, H., Morimura, T., Hanyu, A., Hama, H., Osawa, H., Kashiwagi, S., Fukami, K., Miyata, T., Miyoshi, H., Imamura, T., Ogawa, M., Masai, H., and Miyawaki, A. (2008) Visualizing spatiotemporal dynamics of multicellular cell-cycle progression. *Cell* **132,** 487–498
27. Janssen, A., van der Burg, M., Szuhai, K., Kops, G. J., and Medema, R. H. (2011) Chromosome segregation errors as a cause of DNA damage and structural chromosome aberrations. *Science* **333,** 1895–1898